Van der Waals Complexes in 1,3-Dipolar Cycloaddition Reactions: Ozone-Ethylene

C. W. Gillies,*,† J. Z. Gillies,‡ R. D. Suenram,§ F. J. Lovas,§ E. Kraka,⊥ and D. Cremer⊥

Contribution from the Department of Chemistry, Rensselaer Polytechnic Institute, Troy, New York 12180, Department of Chemistry, Union College, Schenectady, New York 12308, Molecular Physics Division, National Institute of Standards and Technology, Gaithersburg, Maryland 20899, and Theoretical Chemistry, University of Göteborg, Kemigarden 3, S-41296 Göteborg, Sweden. *Received August 8, 1990*

Abstract: Microwave spectra of O_3–CH_2=CH_2, O_3–CD_2=CH_2, O_3–*trans*-CHD=CHD, and O_3–*cis*-CHD=CHD have been observed with a pulsed-beam Fabry–Perot cavity, Fourier transform microwave spectrometer. Internal motions in the van der Waals complex give two states for the normal, 1,1-dideuterated and trans-1,2-dideuterated isotopic forms. The *c*-type transitions of the two states for the isotopic species above, as well as the one observed isotopic form of O_3–*cis*-CHD=CHD, independently fit to an asymmetric top Watson Hamiltonian. Stark effect measurements for O_3–CH_2=CH_2 give μ_a = 0.017 (1) D and μ_c = 0.466 (2) D. The microwave data are only consistent with a structure having C_s symmetry in which the nearly parallel planes of ethylene and ozone have a center of mass separation of R_{cm} = 3.290 (3) Å. Ab initio calculations at the MP4 level indicate that the preferred geometry corresponds to small tilts of the ozone and ethylene planes, which place an exo-oriented pair of hydrogens toward the terminal oxygens of ozone. Both the theoretical and microwave results suggest the tunneling splitting arises at least in part from a 180° rotation of ethylene about its C_2 axis, which is perpendicular to the ethylene plane. 1,3-Dipolar cycloaddition theory, orbital symmetry rules, and ab initio calculations of the complex and transition states are used to argue that O_3–CH_2=CH_2 lies in a shallow minimum on the reaction coordinate prior to the transition state in the reaction of ozone plus ethylene, which produces the primary product 1,2,3-trioxolane.

Introduction

A number of experimental studies have shown that reactant orientation plays an important role in the dynamics of bimolecular gas-phase chemical processes by influencing reaction probabilities and internal state distributions of products. Hexapole fields[1] and photoselection[2] have been used to orient the reacting species. Recently, reactant orientation in the H + CO_2 reaction was achieved by producing the van der Waals CO_2–HBr complex in a nozzle expansion followed by laser photodissociation of the covalent H–Br bond.[3] The same reaction has been studied with the CO_2–HI van der Waals complex as shown in eq 1.[4] In this case, the existence of a collision complex ([OCO–H]) was inferred and its lifetime measured from the delay time of the laser-induced fluorescence signal of the OH product.

$$\text{OCO–HI} \xrightarrow{h\nu} [\text{OCO–H}] + \text{I} \rightarrow \text{CO} + \text{OH} + \text{I} \quad (1)$$

This paper reports a direct approach to the problem of obtaining reactant orientation in a bimolecular gas-phase chemical reaction. Here, a reacting mixture of ethylene and ozone is sampled by a modified pulsed-beam nozzle. The van der Waals complex between the reactants O_3 and C_2H_4 is formed in the expansion and detected in the Fabry–Perot cavity of a Fourier transform microwave spectrometer[5] of the Balle–Flygare type.[6] Both microwave spectral data and ab initio calculations are used to obtain the complex geometry, describe the internal motion, and determine the stability of the complex with respect to ethylene plus ozone. Since the van der Waals complex falls on the reaction potential surface of ozone plus ethylene, the structural results obtained in this research provide detailed structural information about the geometry of a species at large distances along the reaction coordinate. 1,3-Dipolar cycloaddition theory, orbital symmetry rules, and ab initio calculations of the complex and transition state are used to show that the complex lies in a shallow minimum on the reaction coordinate prior to the transition state, which leads to 1,2,3-trioxolane (primary ozonide, $\overline{CH_2OOOCH_2}$), the primary product of the cycloaddition between O_3 and C_2H_4.

Experimental Methods

A Fabry–Perot cavity, Fourier transform microwave spectrometer described previously[5,6] was used to obtain the rotational spectra of the O_3–C_2H_4 complex.[7] Since ethylene reacts rapidly with ozone in the gas phase, mixtures of ~1% ozone in argon and 1% ethylene in argon were independently passed through capillary tubing leading to the high-pressure side of the 0.5-mm orifice of a modified pulsed-solenoid valve.[7,8] Formaldehyde was produced as a product of the ethylene–ozone reaction by means of this flow arrangement. Hence, the pulsed valve serves as a flow reactor as well as a device to sample the reacting gas mixture for spectral analysis in the Fabry–Perot cavity. Two digital flow controllers were used to regulate the gas flows through the pulsed valve. Ozone was prepared by passing molecular oxygen through a Welsbach ozonator into a silica gel trap maintained at dry ice temperature. One of the flow controllers located between a cylinder of compressed argon and the ozone trap regulated the ozone–argon gas flow into the pulsed solenoid valve. The second controller was used to regulate the 1% ethylene in argon through a second gas inlet of the pulsed valve. Gas pulses of 200–400-μs duration from the reacting gas mixture were delivered into the Fabry–Perot cavity at repetition rates up to 35 Hz. Short microwave pulses polarized molecular species in the cavity when the microwave frequency was nearly resonant ($\Delta\nu \leq 0.5$ MHz) with a rotational transition. Free induction emission from the cavity was digitized (512 points, 0.5 μs/point), and typically 200–2000 pulses were averaged. Fourier transforms of the averaged data yielded the power spectrum in the frequency domain

† Rensselaer Polytechnic Institute.
‡ Union College.
§ National Institute of Standards and Technology.
⊥ University of Göteborg.

(1) (a) Brooks, P. R. *J. Chem. Phys.* **1969**, *50*, 5031. (b) Buehler, R. J.; Bernstein, R. B. *J. Chem. Phys.* **1969**, *51*, 5305. (c) Rulis, A. M.; Wilcomb, B. E.; Bernstein, R. B. *J. Chem. Phys.* **1974**, *60*, 2822. (d) Marcelin, G.; Brooks, P. R. *J. Am. Chem. Soc.* **1975**, *97*, 1710. (e) Brooks, P. R. *Science (Washington, D.C.)* **1976**, *193*, 11. (f) Van Den Ende, D.; Stolte, S. *Chem. Phys. Lett.* **1980**, *76*, 13. (g) Stolte, S. *Ber. Bunsen-Ges. Phys. Chem.* **1982**, *86*, 413. (h) Zare, R. *Ber. Bunsen-Ges Phys. Chem.* **1982**, *86*, 422.
(2) (a) Karny, Z.; Estler, R. C.; Zare, R. N. *J. Chem. Phys.* **1978**, *69*, 5199. (b) Rettner, C. T.; Zare, R. N. *J. Chem. Phys.* **1982**, *77*, 2416.
(3) (a) Buelow, S.; Radhakrishnan, G.; Catanzarite, J.; Wittig, C. *J. Chem. Phys.* **1985**, *83*, 444. (b) Radhakrishnan, G.; Buelow, S.; Wittig, C. *J. Chem. Phys.* **1986**, *84*, 727.
(4) Scherer, N. F.; Khundkar, L. R.; Bernstein, R. B.; Zewail, A. H. *J. Chem. Phys.* **1987**, *87*, 1451.
(5) Lovas, F. J.; Suenram, R. D. *J. Chem. Phys.* **1987**, *87*, 2010.
(6) Balle, T. J.; Flygare, W. H. *Rev. Sci. Instrum.* **1981**, *52*, 33.
(7) Gillies, J. Z.; Gillies, C. W.; Suenram, R. D.; Lovas, F. J.; Stahl, W. *J. Am. Chem. Soc.* **1989**, *111*, 3073.
(8) Gillies, J. Z.; Gillies, C. W.; Lovas, F. J.; Matsumura, K.; Suenram, R. D.; Kraka, E.; Cremer, D. *J. Am. Chem. Soc.*, submitted for publication, 1991.

0002-7863/91/1513-2412$02.50/0

Table I. Rotational Transitions of O_3–CD_2=CH_2

transition ($J'_{K_{-1}K_{+1}}$–$J''_{K_{-1}K_{+1}}$)	low-frequency state[a,b] ν_{obsd}[c] (MHz)	low-frequency state[a,b] $\Delta\nu$[d] (kHz)	high-frequency state[a,b] ν_{obsd}[c] (MHz)	high-frequency state[a,b] $\Delta\nu$[d] (kHz)
1_{10}–0_{00}	10105.245	−1	10106.925	6
4_{04}–3_{12}	10245.490	0	10243.940	2
5_{05}–4_{13}	13266.367	0	13264.910	−2
4_{23}–4_{13}	14352.878	−7	14355.980	−9
2_{11}–1_{01}	14919.935	1	14921.610	−5
3_{22}–3_{12}	15213.464	21	15216.567	27
2_{21}–2_{11}	15868.944	−19	15872.054	−5
2_{20}–2_{12}	17234.544	2	17237.633	2
3_{21}–3_{13}	18023.409	−1	18026.455	−1
3_{12}–2_{02}	19966.106	0	19967.763	0

[a] The intensities of the two states are almost the same, which makes it difficult to assign one to the lowest energy state. Most of the lines of the state designated low-frequency are at lower frequency than lines from the second state designated high-frequency. [b] Nuclear spin weight 1. [c] The transition frequencies are estimated to have measurement uncertainties of ~8 kHz. [d] $\Delta\nu$ is the observed minus calculated frequency (kHz) from the least-squares fit.

with a resolution element of 3.9063 kHz/point. The precision and accuracy of the transition frequency measurements for O_3–C_2H_4 lines (15-kHz full widths at half-peak intensity) were estimated to be 4 kHz.

Rotational transitions of Ar–O_3,[9] O_3,[10] and C_2H_4–H_2O[11] were monitored to be certain that both ozone and ethylene were present in the pulsed beam. Optimum signals of the O_3–C_2H_4 complex were obtained at flow rates of 100 cm³/min O_3/Ar and 10 cm³/min C_2H_4/Ar. These signals required the presence of both the ozone and ethylene flows. Formaldehyde lines[12] were observed in the gas pulses by employing the same flow conditions required to see the O_3–C_2H_4 complex. However, spectral lines from the thermally unstable products ethylene primary ozonide,[13] dioxirane,[14] and ethylene secondary ozonide[15] could not be seen in the beam. Deuterium-enriched (99%) samples of CD_2=CH_2, *cis*-CHD=CHD and *trans*-CHD=CHD were used to obtain the spectra of the three dideuterated isotopes of the O_3–C_2H_4 complex.

Results

Spectral Analysis. Accurate spectral predictions are difficult to make for weakly bound complexes, particularly when both monomer subunits are asymmetric tops because the complex geometries are not very certain. Since the ozone plus ethylene reaction leads to ethylene primary ozonide as expected for a 1,3-dipolar cycloaddition,[13] it is reasonable to assume a parallel plane approach of ethylene to ozone (structure A in Figure 1) in the formation of the O_3–C_2H_4 complex. An O_3–C_2H_4 structure with the two parallel planes of ethylene and ozone separated by 3.0 Å and $\theta_1 = \theta_2 = 90°$ predicts a nearly prolate rotor spectrum with intense *c*-type transitions.

The *c*-type 2_{11}–1_{01} and 1_{10}–0_{00} R-branch transitions were found and assigned by Stark effect measurements. Two K_{-1} = 2–1, Q-branch series and three additional R-branch lines completed the *c*-type assignment of O_3–C_2H_4. Each *c*-type transition was accompanied by a satellite line with an intensity about half the intensity of the stronger line. The pairs of transitions are split by 5–10 MHz and have nearly the same Stark effect. A similar doubling of the rotational spectra was observed for the O_3–CD_2=CH_2 and O_3–*trans*-CHD=CHD isotopic species. The intensity ratio of transitions from the two states was about 1/1 for O_3–CD_2=CH_2 as compared to 0.7/1.0 for O_3–*trans*-CHD=CHD. Extensive spectral searches revealed only one set of transitions for the O_3–*cis*-CHD=CHD isotopic species.

Table II. Rotational Transitions of O_3–*cis*-CHD=CHD

transition ($J'_{K_{-1}K_{+1}}$–$J''_{K_{-1}K_{+1}}$)	ν_{obsd}[a] (MHz)	$\Delta\nu$[b] (kHz)
1_{10}–0_{00}	10122.207	26
4_{04}–3_{12}	10371.813	1
5_{24}–5_{14}	13135.435	−5
5_{05}–4_{13}	13383.837	1
4_{23}–4_{13}	14212.344	9
2_{11}–1_{01}	14987.042	−22
3_{22}–3_{12}	15095.010	12
2_{21}–2_{11}	15767.694	−14
2_{20}–2_{12}	17169.784	12
3_{21}–3_{13}	17982.519	−5
3_{12}–2_{02}	20089.802	0

[a] The transitions are estimated to have measurement uncertainties of ~8 kHz. [b] $\Delta\nu$ is the observed minus calculated frequency (kHz) from the least-squares fit.

Table III. Rotational Transitions of O_3–*trans*-CHD=CHD

transition ($J'_{K_{-1}K_{+1}}$–$J''_{K_{-1}K_{+1}}$)	A_1 state[a] ν_{obsd}[c] (MHz)	A_1 state[a] $\Delta\nu$[d] (kHz)	A_2 state[b] ν_{obsd}[c] (MHz)	A_2 state[b] $\Delta\nu$[d] (kHz)
1_{10}–0_{00}	10081.544	0	10079.902	−3
4_{04}–3_{12}	10242.226	0	10243.774	0
5_{24}–5_{14}	13203.374	−5	13200.378	−6
5_{05}–4_{13}			13246.198	0
4_{23}–4_{13}	14262.224	10	14259.213	10
2_{11}–1_{01}	14898.001	0	14896.360	1
3_{22}–3_{12}	15129.613	6	15126.594	3
2_{21}–2_{11}	15790.452	−20	15787.448	−10
2_{20}–2_{12}	17167.855	18	17164.837	0
3_{21}–3_{13}	17964.817	−10	17961.867	9
4_{22}–4_{14}	19159.059	1	19156.156	−6
3_{12}–2_{02}	19948.008	−1	19946.391	1
2_{20}–1_{10}			24999.206	−1

[a] Nuclear spin weight 15. [b] Nuclear spin weight 21. [c] The transitions are estimated to have measurement uncertainties of ~8 kHz. [d] $\Delta\nu$ is the observed minus calculated frequency (kHz) from the least-squares fit.

Table IV. Rotational Constants and Centrifugal Distortion Constants of Ozone–Ethylene Isotopic Species[a]

spectral constant (MHz)	O_3–CD_2=CH_2 low-frequency state	O_3–CD_2=CH_2 high-frequency state	O_3–*cis*-CHD=CHD
A	7697.423 (22)	7699.243 (21)	7689.330 (23)
B	2408.323 (25)	2408.332 (27)	2433.481 (33)
C	1961.439 (33)	1961.451 (36)	1974.958 (52)
Δ_J	0.015 22 (29)	0.015 55 (31)	0.013 73 (23)
Δ_{JK}	0.2056 (14)	0.2062 (15)	0.2465 (22)
Δ_K	−0.2893 (51)	−0.1343 (53)	−0.2380 (46)
δ_J	0.003 13 (15)	0.003 26 (13)	0.002 81 (18)
δ_K	0.152 (13)	0.151 (15)	0.154 (21)

[a] Uncertainties in parentheses are 1 standard deviation from the least-squares fit.

Stark effect measurements were used to assign the two states of O_3–CD_2=CH_2 and O_3–*trans*-CHD=CHD as well as the one state of O_3–*cis*-CHD=CHD. Each state observed for all the isotopic species of the complex was fit separately to an *I*ʳ A-reduced Watson Hamiltonian.[16] The frequency measurements for O_3–CD_2=CH_2 and O_3–*cis*-CHD=CHD are listed in Tables I and II, and those for O_3–*trans*-CHD=CHD are given in Table III. Table IV contains the spectral constants for O_3–CD_2=CH_2 and O_3–*cis*-CHD=CHD. The spectral constants for O_3–*trans*-CHD=CHD are presented in Table V. A preliminary communication contains the transition frequencies and spectral constants for the normal isotopic species O_3–CH_2=CH_2.[7] Table V also lists the spectral constants for O_3–CH_2=CH_2. It is argued in a subsequent section of this paper that the doubling of lines

(9) DeLeon, R. L.; Mack, K. M.; Muenter, J. S. *J. Chem. Phys.* **1979**, *71*, 4487.
(10) Hughes, R. H. *J. Chem. Phys.* **1956**, *24*, 131.
(11) Peterson, K. I.; Klemperer, W. *J. Chem. Phys.* **1986**, *85*, 725.
(12) Lovas, F. J. *J. Phys. Chem. Ref. Data* **1978**, *7*, 1445.
(13) (a) Zozom, J.; Gillies, C. W.; Suenram, R. D.; Lovas, F. J. *Chem. Phys. Lett.* **1987**, *140*, 64. (b) Gillies, J. Z.; Gillies, C. W.; Suenram, R. D.; Lovas, F. J. *J. Am. Chem. Soc.* **1988**, *110*, 7991.
(14) Suenram, R. D.; Lovas, F. J. *J. Am. Chem. Soc.* **1978**, *101*, 5117.
(15) Gillies, C. W.; Kuczkowski, R. L. *J. Am. Chem. Soc.* **1972**, *94*, 6337.
(16) Watson, J. K. G. In *Vibrational Spectra and Structure*; Durig, J. R., Ed.; Elsevier: Amsterdam, 1978; Vol. 6, pp 1–89.

Table V. Rotational Constants and Centrifugal Distortion Contants of Ozone–Ethylene Isotopic Species[a]

spectral constant (MHz)	O_3–CH_2=CH_2[b]		O_3–*trans*-CHD=CHD	
	A_1	A_2	A_1	A_2
A	8246.841 (2)	8241.897 (4)	7673.001 (51)	7671.214 (8)
B	2518.972 (4)	2518.941 (9)	2409.216 (54)	2409.214 (11)
C	2044.248 (5)	2044.287 (11)	1958.598 (37)	1958.581 (13)
Δ_J	0.015 96 (3)	0.015 77 (6)	0.0151 (12)	0.014 768 (68)
Δ_{JK}	0.2333 (2)	0.2350 (4)	0.2116 (20)	0.211 20 (58)
Δ_K	−0.0524 (6)	−0.405 (1)	−0.127 (14)	−0.2813 (19)
δ_J	0.003 16 (2)	0.003 28 (3)	0.002 98 (17)	0.002 955 (51)
δ_K	0.168 (2)	0.147 (5)	0.152 (19)	0.1554 (59)

[a] Uncertainties in parentheses are 1 standard deviation from the least-squares fit. [b] Obtained from Table II in ref 7.

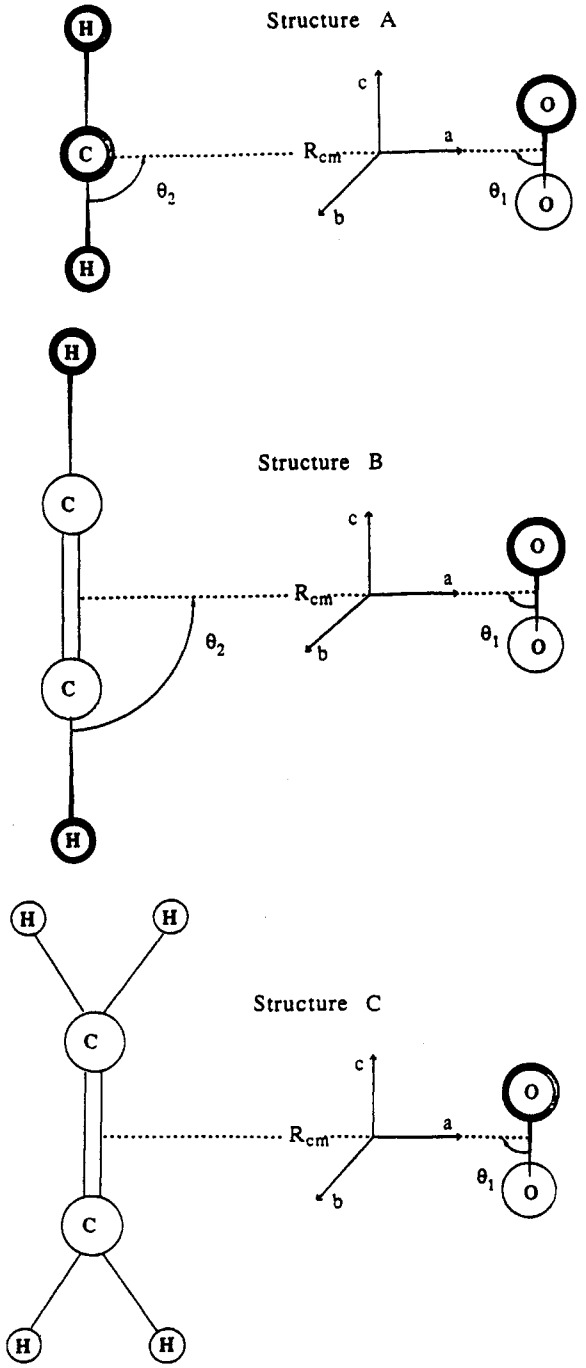

Figure 1. Projections of structures A, B, and C in the *a,c* symmetry plane of O_3–CH_2=CH_2. R_{cm} is the distance of the center of mass of ozone to the center of mass of ethylene, θ_1 is the angle between the local C_2 axis of ozone and R_{cm}, and θ_2 is the angle between R_{cm} and the molecular plane of ethylene.

arises from a tunneling motion, which involves internal rotation of ethylene. The state designations in Tables I–IV are symmetry labels related to this internal motion in the complex.

Table VI. Electric Dipole Moment of Ozone–Ethylene Complex[a]

component (D)	O_3–CH_2=CH_2	O_3
μ_a	0.017 (1)	
μ_c	0.466 (2)	
μ_T	0.466 (2)	0.5324 (24)[b]

[a] The uncertainties given in parentheses are 1 standard deviation of the least-squares fit. All dipole components have units of debye. [b] The total dipole moment $\mu_T = \mu_b$ for free ozone (see ref 12).

Electric Dipole Moment. The frequency shifts as a function of applied electric field were measured for a number of components of O_3–CH_2=CH_2 transitions. As described previously,[17] positive and negative dc voltages were applied to 25 × 25 cm square parallel plates spaced at about 26 cm apart in the cavity. The $\Delta|M_J| = 0$ Stark transitions were observed by orienting the applied dc electric and microwave electric field vectors parallel in the cavity. The effective electric field between the plates was calibrated with use of the $J = 1$–0 transition of OCS and its known dipole moment.[18]

A combination of 25 measurements on the A_1 and A_2 states of O_3–CH_2=CH_2 was used to determine the electric dipole moment of the complex. The Stark effect data include the $|M_J| = 0,1$ components of the 2_{11}–1_{01} transition, the $M_J = 0$ component of the 1_{10}–0_{00} transition, the $|M_J| = 2$ component of the 2_{21}–2_{11} transition and the $|M_J| = 2,3$ components of the 3_{22}–3_{12} transition. Frequency shifts ($\Delta\nu$) of the Stark components were quadratic with respect to the applied electric field.

Linear least-squares fits of the Stark data to second-order perturbation theory[19] gave the results in Table VI. The residual of the fit is 5 kHz with $\mu_a = 0.017$ (1) D and $\mu_c = 0.466$ (2) D. The quality of the fit, as well as the absence of *b*-type transitions, indicates that $\mu_b = 0$. Isotopic moment of inertia data discussed in a subsequent section of this paper confirm the presence of an *a,c* symmetry plane with $\mu_b = 0$ in the complex. The small nonzero value of μ_a derived from the Stark effect data was confirmed by observation of a weak line at 13 576 MHz assigned to the 3_{03}–2_{02} *a*-type transition. Due to the poor signal to noise of 2/1 (5000 pulses at full microwave power) obtained for this transition, no attempts were made to measure additional *a*-type transitions and include them in the spectral least-squares fits.

Structural Analysis. Since μ_b was found to be zero from the electric dipole moment measurements, O_3–CH_2=CH_2 has an *a,c* symmetry plane. The second moment $P_{bb} = {}^1/_2(I_a + I_b)$ is proportional to the square of the out of plane *b* coordinates. For the normal isotopic species, $P_{bb} = 53.94$ uÅ^2 in the A_1 state, which demonstrates that the complex cannot be planar and that a number of heavy atoms are located out of the *a,c* plane. Only three structural forms of O_3–CH_2=CH_2 have heavy atoms out of an *a,c* symmetry plane. Structure A (shown in Figure 1) has four heavy atoms, two terminal oxygens of ozone, and the two ethylene carbons, located symmetrically out of the *a,c* plane. For structures B and C (also shown in Figure 1), the two carbon atoms fall in

(17) Coudert, L. H.; Lovas, F. J.; Suenram, R. D.; Hougen, J. T. *J. Chem. Phys.* **1987**, *87*, 6290.
(18) (a) Muenter, J. S. *J. Chem. Phys.* **1968**, *48*, 4544. (b) Reinhartz, J. M. L. J.; Dymanus, A. *Chem. Phys. Lett.* **1974**, *24*, 346.
(19) Golden, S.; Wilson, E. B. *J. Chem. Phys.* **1948**, *16*, 669.

Table VII. Structural Parameters of Ozone–Ethylene Complex

Monomer Geometry			
O_3[a]	R(O—O) = 1.276 Å		θ(O–O–O) = 116.97°
CH_2=CH_2[b]	R(C=C) = 1.339 Å	R(C—H) = 1.086 Å	θ(H–C–H) = 121.1°

O_3–CH_2=CH_2 geometry	syn a	syn b	anti a	anti b
R_{cm} (Å)	3.291 (3)	3.291 (3)	3.291 (2)	3.291 (3)
θ_1 (deg)	111 (4)	68 (4)	112 (4)	69 (4)
θ_2 (deg)	107 (4)	106 (3)	74 (3)	73 (4)
σ (uÅ^2)	0.39	0.39	0.39	0.39

[a] R(O–O) and θ(O–O–O) were determined from an r_0 fit of the moments of inertia of the normal isotopic species of ozone obtained from rotational constants reported in ref 12. [b] The ethylene r_0 parameters were determined from an r_0 fit in the CH_2=CHD frame with use of the CH_2=CD_2, CH_2=CHD, and *cis*-CHD=CHD second moments P_{aa} and P_{bb} reported by: Hirota, E.; Endo, Y.; Saito, S.; Yoshida, K.; Yamaguchi, I.; Mochida, K. *J. Mol. Spectrosc.* **1981**, *89*, 223.

the *a*,*c* plane while the two terminal oxygens of ozone lie symmetrically out of this plane.

Structure C is not consistent with the moment of inertia data of the three deuterated isotopic species. For structure C, the four hydrogen atoms are located in the *a*,*c* plane, which means that $\Delta P_{bb} = P_{bb}(d_2\text{-isotope}) - P_{bb}(\text{normal isotope}) = 0$. The moment of inertia data determine ΔP_{bb} to be 2.7968, 3.0342, and 3.0315 uÅ^2 for O_3–CD_2=CH_2, O_3–*cis*-CHD=CHD, and O_3–*trans*-CHD=CHD, respectively. These values of ΔP_{bb} for the three deuterated isotopic species show that the deuterium atoms are located symmetrically out of the *a*,*c* plane.

Four heavy atoms are located out of the *a*,*c* plane for structure A, while B has only two heavy atoms out of this plane. Hence, a comparison of calculated values of P_{bb} with the experimental value for the normal isotopic species provides a way to distinguish A from B. The geometries of free ozone and ethylene listed in Table VII were used to calculate P_{bb} for the two forms. The center of mass separation (R_{cm}) and the angles θ_1 and θ_2 shown in Figure 1 do not affect the calculated values of P_{bb} because the out of plane *b* coordinates are not functions of these parameters. Structures A and B have calculated values of P_{bb} = 54.68 and 41.38 uÅ^2, respectively. P_{bb} for structure A is in excellent agreement with the value of 53.94 uÅ^2 determined from the experimental rotational constants of the A_1 state. Structure B has a much lower calculated P_{bb}, as expected for a geometry with only two heavy atoms located out of the *a*,*c* plane. In summary, the electric dipole moment and moment of inertia data are consistent only with structure A, which has C_s symmetry.

If the monomer geometries are not changed by complexation, R_{cm} (the center of mass separation), θ_1 (the angle between R_{cm} and the local C_2 axis of ozone), and θ_2 (the angle between R_{cm} and the molecular plane of ethylene) are required to determine the geometry of structure A (see Figure 1). The isotopic spectral data of the complex include effective rotational constants of two states for O_3–CH_2=CH_2, O_3–CD_2=CH_2, and *trans*-CHD=CHD. In a subsequent section of this paper, these states are rationalized in terms of a tunneling motion through a barrier that involves internal rotation of ethylene. Differences between the effective rotational constants of the two states for each isotopic species are small. The structural determination used effective rotational constants from the ground A_1 state.

In the case of O_3–*cis*-CHD=CHD, the internal motion does not give rise to two tunneling states. However, two different structural isotopic species of O_3–*cis*-CHD=CHD are possible for structure A with C_s symmetry. These forms are designated *anti*-(O_3–*cis*-CHD=CHD) and *syn*-(O_3–*cis*-CHD=CHD). Experimentally only one form is seen in the supersonic expansion. This form is likely the lower energy species because extensive spectral searches did not reveal the presence of a second set of rotational transitions. In the SO_2–CH_2=CH_2 complex, which has a similar structure with C_s symmetry and analogous internal motions, two structural forms of SO_2–*cis*-CHD=CHD were observed with use of a helium carrier gas in the supersonic expansion as a means of producing a warmer beam.[20] This was not possible in the ozone–ethylene complex due to the lower overall intensity of the spectrum.

Table VIII. Comparison of Chutjian Substitution Coordinates with r_0 Coordinates for Hydrogen in Ozone–Ethylene Complex

atomic coordinate (Å)	*a*	*b*	*c*
hydrogen (substitution)[a]	1.6931	1.2352	0.8504
hydrogen r_0 (syn a)[b]	−1.8084	∓1.2305	+0.8831
hydrogen r_0 (syn b)	−1.8068	∓1.2305	+0.9185
hydrogen r_0 (anti a)	−1.8068	∓1.2305	−0.9185
hydrogen r_0 (anti b)	−1.8084	∓1.2305	−0.8831

[a] The magnitude but not the sign of the atomic coordinates is determined by Chutjian's equations (see ref 21). The coordinates were obtained with use of the normal isotopic species as the parent and O_3–*cis*-CHD=CHD for the substituted species. [b] The r_0 coordinates for hydrogen are obtained from the moment fits summarized in Table VII.

The observation of only one form of O_3–*cis*-CHD=CHD makes it difficult to assign the effective rotational constants obtained from the spectral analysis to the anti or syn isotopic species. This problem is due to the similarity of the magnitude of the syn and anti deuterium coordinates. Least-squares fits of the moment of inertia data require an assignment of the observed O_3–*cis*-CHD=CHD isotopic species to either the anti or syn form. Hence, two structural fits were carried out with use of the anti assignment in one and the syn assignment in the other.

Since R_{cm}, θ_1, and θ_2 are dependent upon $P_{aa} = {}^1/_2(I_b + I_c - I_a)$ and $P_{cc} = {}^1/_2(I_a + I_b - I_c)$ but not P_{bb}, only P_{aa} and P_{cc} for the four isotopic species were used in the least-squares fits. In these fits, the monomer ozone and ethylene geometries were fixed at the r_0 values listed in Table VII. Table VII also gives R_{cm}, θ_1, and θ_2 obtained from the fits for the *syn*- and *anti*-(O_3–*cis*-CHD=CHD) assignments. Fits involving both syn and anti assignments of the O_3–*cis*-CHD=CHD isotopic species are equally compatible with supplementary angles of 68° and 112° for θ_1. However, the syn assignment fit determines θ_2 to be 106°, while the supplementary angle of 74° for θ_2 is found with the fit that assigns the O_3–*cis*-CHD=CHD isotopic species to the anti form.

The combination of the ambiguity in the assignment to the syn or anti forms of O_3–*cis*-CHD=CHD and the lack of oxygen-18 isotopic substitution required to distinguish θ_1 = 68° from θ_1 = 112° leaves four geometries consistent with the observed moment of inertia data. All four fits listed in Table VII determine R_{cm} to be 3.290 (3) Å. However, the ethylene and ozone planes are tilted ±16° and ±22°, respectively, from the parallel plane θ_1 = θ_2 = 90° structure shown as structure A in Figure 1. These four structures are illustrated in Figure 2.

Chutjian's double substitution equations give the hydrogen coordinates for the observed form of O_3–*cis*-CHD=CHD.[21] Table VIII compares these substitution coordinates with the syn and anti hydrogen coordinates calculated from the fits given in Table VII. Unfortunately, only the *c* hydrogen coordinate differs among the syn and anti forms. Furthermore, supplementary angles for θ_1 and θ_2 are obtained in the syn a, anti b and syn b, anti a pairs of fits. As shown in Table VIII, this leads to *c* hydrogen coordinates, which are equal in magnitude but opposite in sign for each of the two pairs of fits. Since Chutjian's substitution method does not give the signs of the atomic coordinates, it is not possible to distinguish the *syn*- and *anti*-(O_3–*cis*-CHD=CHD) isotopic assignment. The magnitudes of the *c* hydrogen coordinates do not differ greatly between the two pairs of fits. However, a little better agreement is found between the magnitude of the *c* hydrogen coordinates determined for the syn b, anti a pair and the substitution value of 0.8504 Å.

Internal Motions. The two tunneling states observed for O_3–CH_2=CH_2, O_3–CD_2=CH_2, and O_3–*trans*-CHD=CHD

(20) (a) LaBarge, M. S.; Hillig, K. W., II; Kuczkowski, R. L. *Angew. Chem., Int. Ed. Engl.* **1988**, *27*, 1356. (b) Andrews, A. M.; Taleb-Bendiab, A.; LaBarge, M. S.; Hillig, K. W., II; Kuczkowski, R. L. *J. Chem. Phys.* **1990**, *93*, 7030.

(21) Chutjian, A. *J. Mol. Spectrosc.* **1964**, *14*, 361.

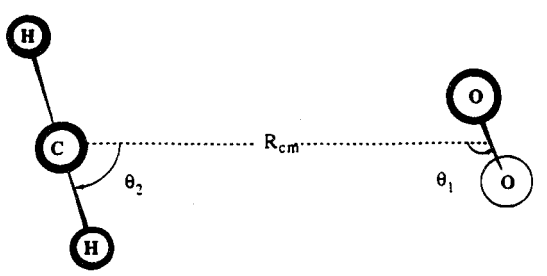

anti **a**: θ_1=112°, θ_2=74°, R_{cm}=3.291Å

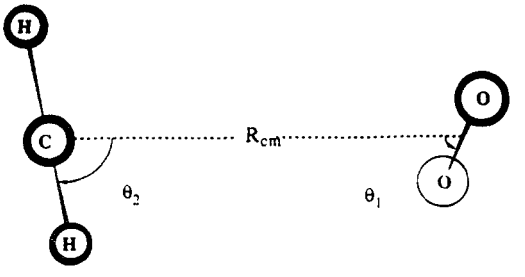

anti **b**: θ_1=69°, θ_2=73°, R_{cm}=3.291Å

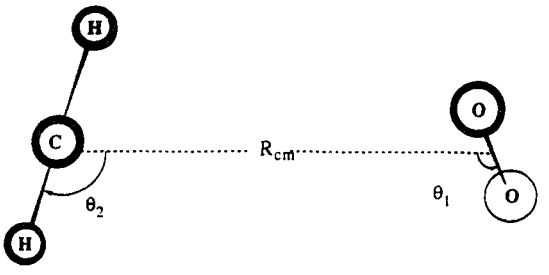

syn **a**: θ_1=111°, θ_2=107°, R_{cm}=3.291Å

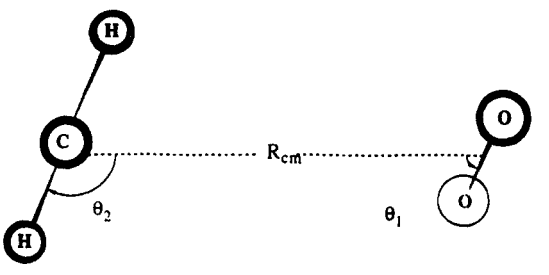

syn **b**: θ_1=68°, θ_2=106°, R_{cm}=3.291Å

Figure 2. Conformations designated anti a, anti b, syn a, and syn b obtained from the least-squares fits of second moments of inertia of ozone–ethylene complex isotopic species.

likely arise from a motion that exchanges equivalent pairs of hydrogen and/or deuterium atoms in ethylene, i.e., internal rotation of ethylene about one of its C_2 symmetry axes. An inversion motion of ozone reverses the direction of the dipole moment of ozone along the *c* principal axis of the complex, which gives *c*-type rotation–inversion transitions. Since the *c*-type transitions fit to within the experimental uncertainty of the frequency measurements to a standard Watson Hamiltonian, there is no evidence that an inversion of ozone is the origin of the tunneling states.

There are three different internal rotations of ethylene. As shown in Figure 3, 180° rotation about each of the C_2 axes in ethylene exchanges two pairs of equivalent hydrogen atoms. Since two tunneling states are observed, only one of these three internal motions are possible. On the basis of a complex having C_s symmetry, each of the three internal rotations produces two equilibrium frameworks. For each internal rotation, the permutation inversion operation to be applied upon the wave function of framework 1 is given under that framework in Figure 3. The permutation inversion group for each internal rotation of ethylene is isomorphic to the C_s symmetry group. This means each asymmetric rotor level is split into two components and the symmetry species of these components are A_1 and A_2. The allowed transitions are A_1–A_1 and A_2–A_2, which give rise to two sets of lines designated A_1 and A_2.

Exchange of the two pairs of hydrogens in O_3–CH_2=CH_2 gives nuclear spin statistical weights of g = 10 and g = 6 for the A_1 and A_2 states, respectively. This produces an intensity ratio of 10/6 = 1.67 for a given transition pair arising from the A_1/A_2 states, respectively. Since all three possible internal rotations of ethylene exchange two pairs of hydrogens, the 10/6 nuclear spin weighting of the A_1/A_2 states is expected for all of these internal motions shown in Figure 3. Relative intensity measurements show the set of lines designated "ground state" in Table I of ref 7 is a factor of 1.6 more intense than the set of lines designated "excited state" in the same reference. The good agreement between the measurements of the relative intensities and the intensities predicted by nuclear spin statistics supports the assignment of the tunneling motion to an internal rotation of ethylene, which exchanges the hydrogen pairs. From the observed relative intensities, it is possible to assign the A_1 state to the more intense "ground state" lines and the A_2 state to the less intense "excited state" lines. This tunneling state designation is employed for the spectral constants of O_3–CH_2=CH_2 listed in Table V.

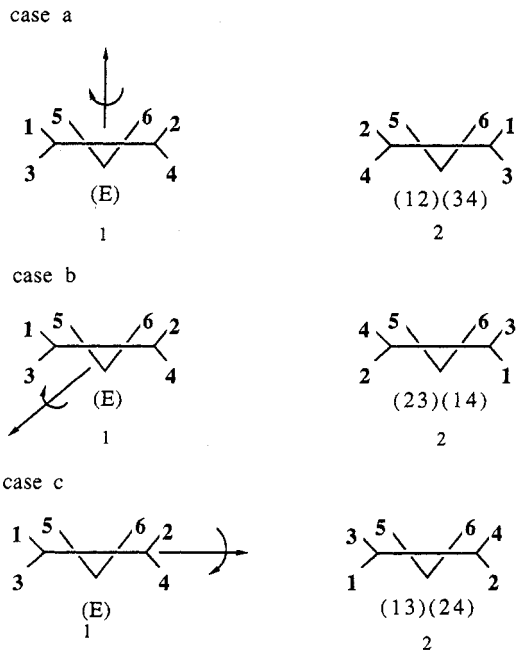

Figure 3. Nonsuperimposable frameworks of O_3–CH_2=CH_2 projecting the complex approximately in the *b*,*c* plane. Cases a, b, and c refer to the three different internal rotations of ethylene. Two equilibrium frameworks designated 1 and 2 are possible for each of the three internal rotations, and the permutation inversion operation to be applied upon the basis function of framework 1 is given in parentheses under that framework. 1, 2, 3, and 4 represent hydrogen atoms in ethylene, while 5 and 6 denote oxygen atoms in ozone.

Nuclear spin statistics and measurements of relative intensities of lines from the two tunneling states in O_3–CD_2=CH_2 and O_3–*trans*-CHD=CHD can be used to determine the axis of rotation in ethylene that causes the tunneling splitting of the transitions. Since the moments of inertia and electric dipole data show that the complex has C_s symmetry, only one structural isomer is possible for both O_3–CD_2=CH_2 and O_3–*trans*-CHD=CHD. The two tunneling states observed for each of these isotopic species have different nuclear spin statistical weights depending upon which local C_2 axis of rotation is involved in the internal motion. In case a, 180° rotation about the C_2 axis perpendicular to the C=C axis and lying in the plane of ethylene, i.e., the *b* inertial axis of ethylene, does not lead to equivalent frameworks for either O_3–CD_2=CH_2 or O_3–*trans*-CHD=CHD (see Figure 3); hence, $g = 1$ for both of the tunneling states of these two isotopic species. In case b, the internal rotation gives equivalent frameworks for O_3–*trans*-CHD=CHD but not for O_3–CD_2=CH_2. Therefore, nuclear spin weights of $g = 15$ and $g = 21$ are required for the A_1 and A_2 states, respectively, of O_3–*trans*-CHD=CHD, while $g = 1$ for both states of O_3–CD_2=CH_2. A 180° rotation about the C=C axis of ethylene for case c results in the converse of case b; i.e., nuclear spin weights of $g = 15$ and 21 are expected for the A_1 and A_2 states of O_3–CD_2=CH_2, while $g = 1$ for both states of O_3–*trans*-CHD=CHD.

Averages of intensity ratio measurements of pairs of a given rotational transition from the two tunneling states give 0.97 and 0.68 for O_3–CD_2=CH_2 and O_3–*trans*-CHD=CHD, respectively. These ratios are in good agreement with the values of 1.0 and 0.71 obtained from nuclear spin statistical weights for case b. Therefore, the relative intensity data indicate that the tunneling states arise from internal rotation about the C_2 axis that is perpendicular to the molecular plane of ethylene. The tunneling state designations of the sets of lines for O_3–CD_2=CH_2 and O_3–*trans*-CHD=CHD in Tables I and III were obtained from the intensity measurements and nuclear spin statistical weights.

With C_s symmetry, two different structural isomers are possible but were not observed for O_3–*cis*-CHD=CHD (see structure section of this paper). Only the internal rotation of ethylene illustrated as case a in Figure 3 leads to equivalent frameworks for O_3–*cis*-CHD=CHD. Hence, only this tunneling motion exchanges the deuteriums and hydrogens to give two tunneling states. Note that the internal rotations described by cases b and c cannot give two tunneling states for O_3–*cis*-CHD=CHD because the rotations give a different structural isomer. Consequently, the absence of two tunneling states for O_3–*cis*-CHD=CHD is consistent with an internal rotation about the C_2 axis that is perpendicular to the molecular plane of ethylene (case b).

For both O_3–CD_2=CH_2 and O_3–*trans*-CHD=CHD, the nuclear spin of each deuterium is 1, which leads to a symmetry-state dependence of the deuterium nuclear electric quadrupole interaction.[22] There must be a distinct difference in the quadrupole hyperfine structure of rotational lines arising from the two isotopic species that depends upon the axis of internal rotation in ethylene. Observation of these hyperfine effects can be used to independently determine the axis of rotation and confirm the conclusions obtained from the relative intensity measurements.

For case b in Figure 3, the tunneling motion exchanges the two deuterium nuclei for O_3–*trans*-CHD=CHD but not O_3–CD_2=CH_2, which makes the two deuterium nuclei equivalent in O_3–*trans*-CHD=CHD. These two equivalent deuterium nuclei are coupled to each other to give $I_1 + I_2 = I_D$, where $I_D = 0$, 1, and 2. I_D couples to the complex rotational framework so that $J + I_D = F$. The pairs of equivalent deuterium and hydrogen nuclei have spin 1 and $^1/_2$, respectively, and obey Fermi–Dirac statistics in O_3–*trans*-CHD=CHD for the tunneling motion in case b of Figure 3. Thus, the symmetric A_1 state wave function combines with the antisymmetric $I_D = 1$ spin wave function, while the antisymmetric A_2 state wave function is combined with $I_D = 0,2$ symmetric spin wave functions. Because of the tunneling motion, only one quadrupole coupling constant characterizes the two deuterium nuclei. Furthermore, the hyperfine structure of a given rotational transition for the A_1 state will differ markedly from the A_2 state due to the absence of the $I_D = 1$ components. This is analogous to the $^{14}N_2$–H_2O complex, where analysis of the hyperfine components demonstrated $\chi(^{14}N)$ is the same in the tunneling states due to the exchange of the two ^{14}N nuclei.[22]

The two deuterium nuclei in O_3–CD_2=CH_2 are not exchanged by the tunneling motion for case b in Figure 3, and all the nuclear spin states ($I_D = 0,1,2$) are allowed for each rotational level of the A_1 and A_2 tunneling states. Consequently, the complete set of hyperfine components will be present for each transition. Since the two quadrupole coupling constants are expected to be quite similar for the A_1 and A_2 states, the hyperfine structure will be similar for a given rotational transition arising from the A_1 and A_2 states of O_3–CD_2=CH_2.

There is not a sufficient number of resolved hyperfine components in the transitions of O_3–*trans*-CHD=CHD and O_3–CD_2=CH_2 to obtain the state *F* labels and the quadrupole coupling constants. However, the 1_{10}–0_{00} transition clearly shows that the hyperfine structure is almost identical for the A_1 and A_2 states of O_3–CD_2=CH_2, while the A_1 and A_2 states of O_3–*trans*-CHD=CHD have distinctly different hyperfine structure. Figure 4 compares the two 1_{10}–0_{00} transitions arising from the A_1 and A_2 states of O_3–CD_2=CH_2 and O_3–*trans*-CHD=CHD. The tunneling motion shown in Figure 3 as case c will lead to the opposite hyperfine structure expected in case b for the two isotopes. This is because the 180° rotation exchanges the deuterium nuclei in O_3–CD_2=CH_2 but not in O_3–*trans*-CHD=CHD. Since the tunneling motion in case a does not exchange the deuterium nuclei in either isotopic species, the hyperfine structures of the A_1 and A_2 states will be similar in each isotopic species. Therefore, the observed hyperfine structure for the A_1 and A_2 states of O_3–*trans*-CHD=CHD and O_3–CD_2=CH_2 is consistent only for the tunneling motion described in Figure 3 as case b, which supports the conclusion drawn from the relative intensity measurements, i.e., *rotation of ethylene about the axis perpendicular to its plane.*

Only the *A* rotational constant and Δ_K differ significantly between the tunneling states in O_3–CH_2=CH_2, O_3–CD_2=CH_2, and O_3–*trans*-CHD=CHD. The internal rotation axis of ethylene perpendicular to its molecular plane falls almost along the *a* inertial axis of the complex. This can be seen qualitatively in Figure 2 for the syn a form, where the *a* axis of the complex is located approximately along R_{cm} and $\theta_2 = 106°$ places the internal rotation axis at approximately a 16° angle with respect to the *a* inertial axis. This means that the *b* and *c* coordinates of the complex and consequently the *A* rotational constant will be primarily affected by the tunneling motion. Although Δ_K does not have a simple interpretation in terms of the principal axes coordinates, it is closely related to the *A* rotational constant.

It is important to note that the tunneling motion may also involve ozone and still be consistent with the observed spin weights and nuclear quadrupole hyperfine structure as long as the ozone motion does not involve an inversion of the dipole moment along the *a* and *c* inertial axes. For example, a gearlike internal rotation of ozone coupled to the internal rotation of ethylene also exchanges the equivalent terminal oxygen atoms of ozone. Since the nuclear spin of oxygen nuclei is zero and oxygen has no nuclear electric quadrupole moment, this gearlike motion will lead to two tunneling states with the same nuclear spin weights and nuclear quadrupole structure expected for a tunneling motion that only involves internal rotation of ethylene. The tunneling splitting should be less sensitive to deuteration of ethylene for a concerted gearlike motion involving both ethylene and ozone due to the larger, reduced mass associated with the motion. Although deuteration of ethylene in O_3–C_2H_4 does generally reduce the tunneling splitting by a factor of 2–3 (for example, compare the tunneling splitting for O_3–*trans*-CHD=CHD in Table III with O_3–CH_2=CH_2 in Table I of ref 7), it does not exclude some contribution from ozone to the tunneling motion.

Theoretical Results. Various levels of theory ranging from Hartree–Fock (HF) to fourth-order Moller–Plesset (MP) per-

(22) Leung, H. O.; Marshall, M. D.; Suenram, R. D.; Lovas, F. J. *J. Chem. Phys.* **1989**, *90*, 700.

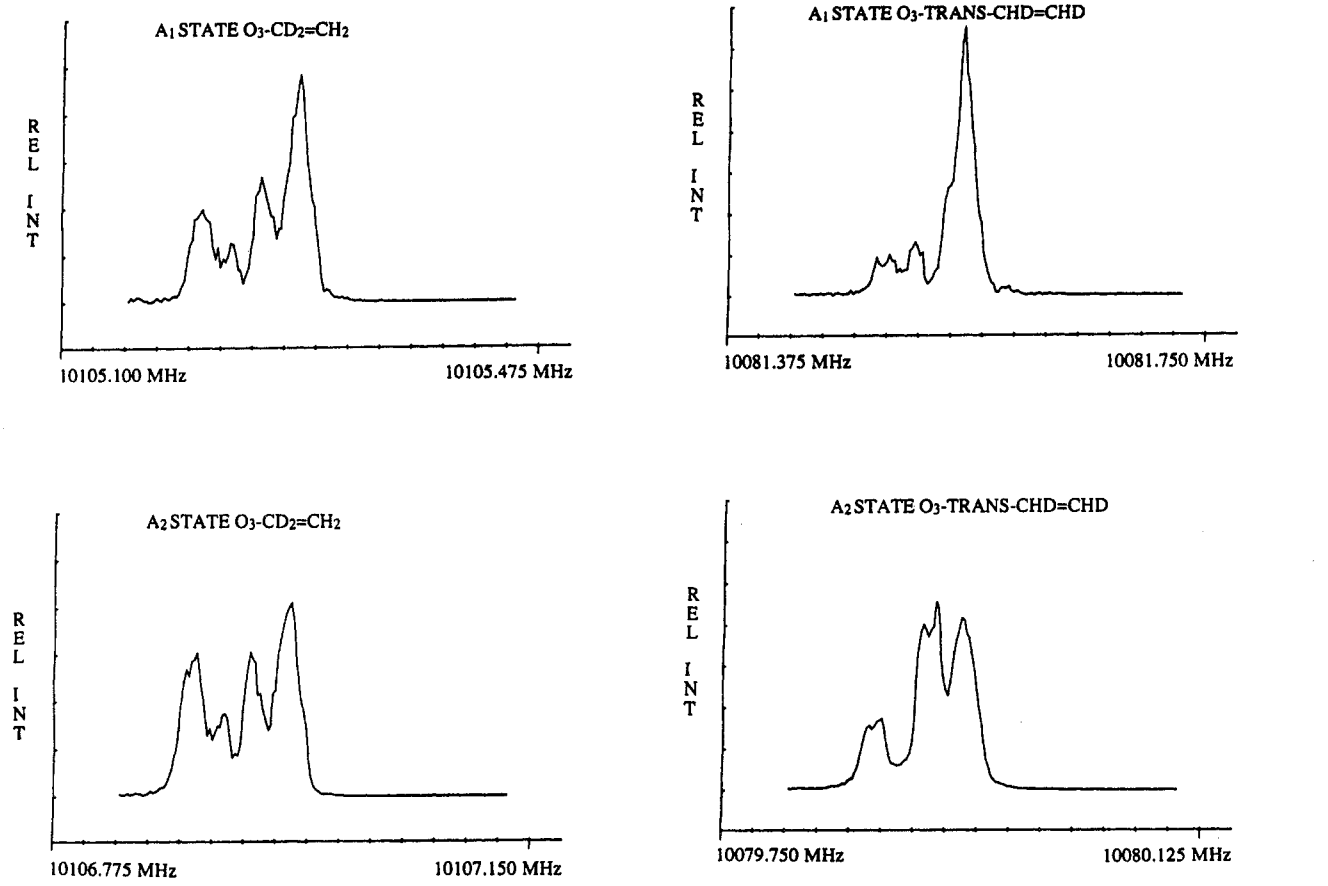

Figure 4. 1_{10}–0_{00} *c*-type transitions of the two tunneling states of O_3–CD_2=CH_2 and O_3–*trans*-CHD=CHD illustrating the deuterium quadrupole hyperfine components. The frequency markers are at 25-kHz intervals. Beam expansion conditions were chosen such that Doppler splitting was eliminated.

turbation theory with single (S), double (D), triple (T), and quadruple (Q) excitations [MP4(SDTQ)][23] have been used to investigate the O_3–C_2H_4 complex, computationally. Three different basis sets have been tested, namely, the 6-31G(d,p), 6-311G(d,p), and 6-31G(2d,p) basis sets,[24] which are of DZ + P, TZ + P, and DZ + 2P quality in the valence shell. It is known that a reliable description of weakly bound van der Waals complexes requires basis sets of TZ + P quality and a method that covers correlation effects to a large extent. In this research, it was not feasible to use the two larger basis sets at the highest level of theory. However, the overall description of the complex at the MP4/6-31G(d,p) level of theory is rather useful when combined with the results of the microwave investigation.

In the first step, the energies of the four forms shown in Figure 2 have been calculated. Utilizing the parameters R_{cm}, θ_1, and θ_2 given in Figure 2 allows the energies summarized in Table IX to be obtained. At all levels of theory, the syn a form turns out to be most stable. According to MP4(SDTQ) calculations, the anti a form is 0.4 kcal/mol less stable, while the anti b and syn b forms are 1.0 and 1.2 kcal/mol higher in energy than the syn a form (Table IX).

Analysis of the calculated wave functions reveals that, in the syn a form, electrostatic attraction between the positively charged H atoms of ethylene and the negatively charged terminal O atoms of ozone is more pronounced than in any of the other three forms. In particular, the exo positioned H atoms are closer to the terminal O atoms in the syn a form than in syn b or the anti forms. This leads to an induced dipole moment for ethylene that contributes to the stability of the π complex by dipole-induced dipole attraction. If π–π overlap was the most important factor in the stability of the complex, then the molecular planes of ozone and ethylene would be parallel ($\theta_1 = \theta_2 = 90°$). In the syn a and the anti b forms, the π orbitals deviate from parallel alignment by about 40°, while the deviation is just 5° in the case of the anti a and syn b forms. However, in the latter forms, the lateral displacement between the π orbitals at the C and the terminal O atoms is almost 1 Å and, therefore, π overlap is not a significant factor in any of the four forms considered here. This is in line with the fact that π overlap between C and O at a distance of 3.3 Å is less than 0.01 Å. Hence, factors that increase electrostatic attraction between ozone and ethylene dominate the stability of the complex.

After the preferred conformation of the O_3–C_2H_4 complex is established, its geometry has been calculated directly at the HF, MP2, MP4(SDQ), and MP4(SDTQ) levels of theory with recently developed analytical gradients for MP4.[25] Results of these calculations are listed in Table X. The HF/6-31G(d,p) and

Table IX. Calculated Energies of the Anti and Syn Forms (See Figure 2) as Obtained at Various Levels of Theory by Employing the 6-31G(d,p) Basis Set[a]

method	syn a	anti a	syn b	anti b
HF	−302.285 64	0.45	0.40	0.50
MP2	−303.207 30	0.40	1.75	1.50
MP3	−303.185 68	0.40	1.24	1.09
MP4(SDQ)	−303.208 98	0.42	0.95	0.83
MP4(SDTQ)	−303.261 40	0.41	1.23	1.04

[a] For the syn a form, absolute energies are given in hartrees; for the other forms, relative energies are given in kilocalories per mole relative to the energy of the syn a form.

(23) (a) Krishnan, R.; Pople, J. A. *Int. J. Quantum Chem.* **1978**, *14*, 91. (b) Krishnan, R.; Frisch, M. J.; Pople, J. A. *J. Chem. Phys.* **1980**, *72*, 4244.
(24) (a) Hariharan, P. C.; Pople, J. A. *Chem. Phys. Lett.* **1972**, *66*, 217. (b) Krishnan, R.; Binkley, J. S.; Seeger, R.; Pople, J. A. *J. Chem. Phys.* **1980**, *72*, 650.
(25) Gauss, J.; Cremer, D. *Chem. Phys. Lett.* **1988**, *150*, 280; **1988**, *153*, 303.

Table X. Comparison of Calculated and Experimental Geometries of O_3–C_2H_4[a]

parameter	HF 6-31G(2d,p)	MP2[b] 6-31G(d,p)	MP4(SDQ) 6-31G(d,p)	MP4(SDTQ) 6-31G(d,p)	exptl[c] r_0	r_e[d] (O_3, C_2H_4)
R(OO)	1.196	1.324	1.269	1.306	(1.276)	1.276
R(CC)	1.316	1.347	1.336	1.339	(1.339)	1.330
R(C–H_{endo})	1.076	1.080	1.081	1.082	(1.086)	1.076
R(C–H_{exo})	1.076	1.079	1.080	1.082	(1.086)	1.076
θ(O–O–O)	118.9	114.1	117.4	117.2	(117.0)	116.8
θ(C–C–H_{endo})	121.7	121.5	121.7	121.7	(121.1)	121.7
θ(C–C–H_{exo})	121.7	121.3	121.7	121.7	(121.1)	121.7
R	3.523	2.425	3.048	2.984	3.216	
α_1	85.5	113.2	105.9	112.7	107.6	
α_2	108.0	94.0	102.7	108.9	110.7	
α_3	72.0	90.6	77.5	71.1	69.3	

[a] Distances R are given in Angstroms, angles α in degrees. [b] Reference 26a. [c] Assumed r_0 values taken from the experimental geometry of either ethylene or ozone (see Table VII) are indicated by parentheses. [d] Experimental r_e geometries: O_3, Tanaka, T.; Morino, Y. *J. Mol. Spectrosc.* **1970**, *33*, 538; C_2H_4, Kuchitsu, K. *J. Chem. Phys.* **1966**, *44*, 906.

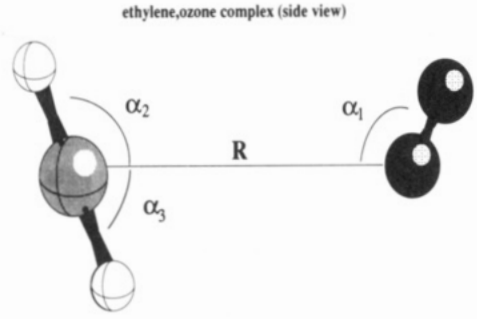

Figure 5. Definitions of the structural parameters R, α_1, α_2, and α_3 used in the ab initio calculations. A side view of ethylene (left) and ozone (right) is shown. R is the distance between the center of the C=C bond and the midpoint between the terminal O atoms of ozone. α_1 is defined as the angle between the distance R and the C_2 axis of ozone. α_2 and α_3 are the angles between R and the local C_2 axes of the two HC=CH entities of ethylene. Note that the two HC=CH entities are no longer in one plane if interactions with ozone lead to a pyramidalization at the C atoms.

MP2/6-31G(d,p) results have been published before by McKee and Rohlfing.[26]

The parameters R, α_1, α_2, and α_3 rather than R_{cm}, θ_1, and θ_2 have been used to describe the conformation of the complex. The distance R is the distance between the midpoint of the C–C bond and the midpoint between a line connecting the terminal O atoms. The angles α_1, α_2, and α_3 are defined with respect to this line as is shown in Figure 5. HF and MP2 values of R differ considerably from the experimental value also given in Table X. HF overestimates the intermolecular distance R by 0.3 Å, while MP2 underestimates R by 0.8 Å.

This is one of the few cases where the MP2 result is worse than that obtained at the HF level. Test calculations with the 6-311G(d,p) and the 6-31G(2d,p) basis sets show that the value of R is due to deficiencies of MP2 and, therefore, R does not improve with larger basis sets. The reason for this failure at the MP2 level can be seen by comparing the calculated dipole moment (μ) of ozone: (HF/6-31G(d,p), 0.83; MP2/6-31G(d,p), 0.16; MP4(SDQ)/6-31G(d,p), 0.56; and MP4(SDTQ)/6-31G(d,p), 0.44 D) with the experimental one (0.53 D, see Table VI). The HF value of μ is too large by 60%, which is due to the fact that HF overestimates the polarity of the O–O bond in ozone. As a consequence, electrostatic interactions between ozone and ethylene come out too large at the HF level, thus leading to a large value of the intermolecular distance R.

The reverse is true at the MP2 level: MP2 mixes too much biradical character into the ozone wave function, which underestimates the charges at the O atoms and predicts a μ value 70% too small. Hence, at the MP2 level, O_3 and C_2H_4 have to come rather close together in order to form a stable complex. Accordingly, the geometries of the two interacting molecules change much more at the MP2 level than at the HF level. This is evident from the calculated small pyramidalization at the C atoms reflected by $\alpha_2 + \alpha_3 = 184.6$ at the MP2 level in Table X.

Reliable predictions of the complex geometry are only possible at the MP4 level of theory, where in view of the calculated values of the ozone dipole moment, MP4(SDQ) seems to be better than MP4(SDTQ). This is confirmed by the results given in Table X, which show that MP4(SDQ) provides a somewhat better description of both the monomers and the complex. The calculated MP4(SDQ) value of R is 0.17 Å too short, and the angles α_1 and α_2 are 2° and 8° too small. On the other hand, MP4(SDTQ) leads to a little better agreement with experimental α values but predicts R 0.23 Å too short. Test calculations with the 6-31G-(2d,p) and 6-311G(d,p) basis sets indicate that these deviations are due to basis set rather than method deficiencies.

The geometry obtained at the MP4 level confirms that the syn a form is the most stable conformation of the O_3–C_2H_4 complex. Furthermore, the calculated MP4 energy provides an estimate of the stability of the complex. At MP4(SDTQ)/6-31G(d,p), the complex is more stable by 2.1 kcal/mol than the separated molecules ozone and ethylene. Since the employed basis set is rather small, corrections for the basis set superposition error (BSSE) are important. Utilizing the counterpoise method[27] for ozone and ethylene allows the stability of the O_3–C_2H_4 complex to be found to be 0.74 kcal/mol.

Since the internal motion that gives rise to the tunneling splitting in the rotational spectrum of O_3–C_2H_4 likely involves internal rotation of ethylene, we have investigated the barriers and transition-state geometries for the three different internal rotation pathways shown in Figure 3. Assuming rigid rotation, i.e., fixing the geometry of ozone and ethylene at the experimental values listed in Table VII, barriers of 8.31, 0.37, and 2.92 kcal/mol are calculated at the MP4(SDTQ)/6-31G(d,p) level for cases a, b, and c, respectively. Optimization of R and the α angles for the transition states reveals that the two monomers separate in case a for a rotation about the C_2 axis located in the plane of ethylene perpendicular to the C=C axis, while ethylene swings into the plane of ozone ($\alpha_1 = 180°$) for rotation about the C=C axis of ethylene (case c). A true transition state for internal rotation is obtained only for case b. This is in agreement with the observed spin weights and nuclear hyperfine splitting, which indicates that the internal rotation is about the C_2 axis perpendicular to the molecular plane of ethylene.

Discussion

Structure and Internal Dynamics. The ab initio calculations have found that, of the four forms in Figure 2 consistent with the microwave spectral data, the syn a structure is the most stable. Since $\theta_1 = 112°$ and $\theta_2 = 106°$, the two monomer planes are not parallel for the syn a form and the C–$O_{terminal}$ distances equal 3.24 Å. The best ab initio result obtained in this research predicts the stability of the complex to be 0.74 kcal/mol.

(26) (a) McKee, M. L.; Rohlfing, C. M. *J. Am. Chem. Soc.* **1989**, *111*, 2497. (b) Cremer, D.; McKee, M. L. To be published.

(27) Boys, F.; Bernardi, F. *Mol. Phys.* **1970**, *19*, 553.

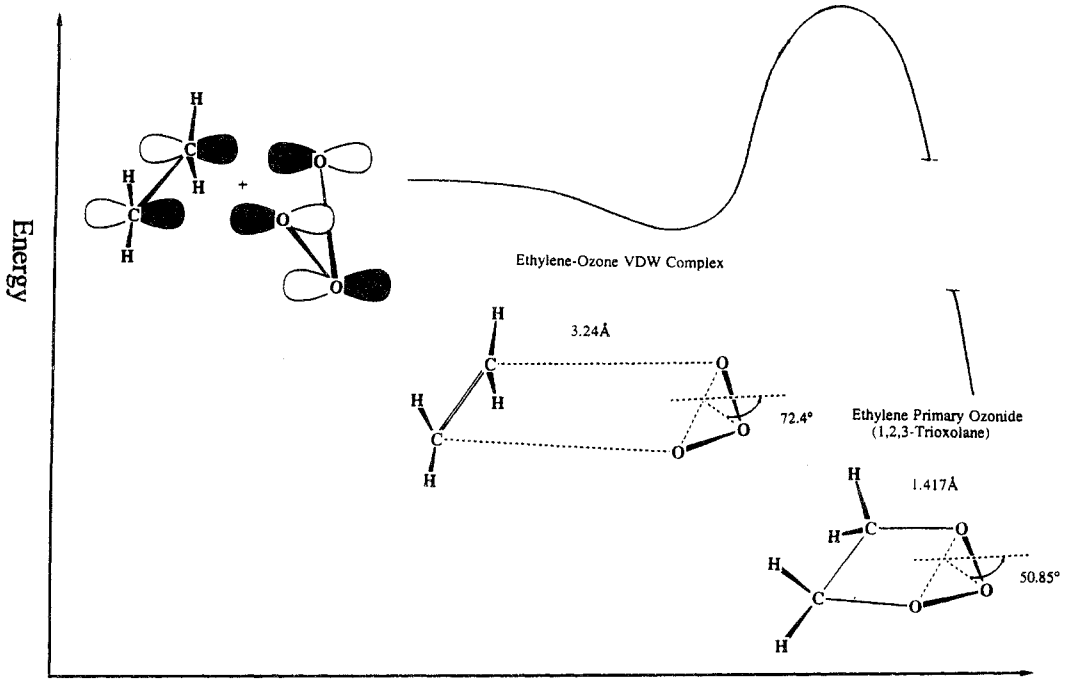

Figure 6. One-dimensional reaction potential surface of ozone plus ethylene defined by 1,3-dipolar cycloaddition theory.

Table XI. Van der Waals Stretching Frequencies (ω_s), Force Constants (k_s), Radii Sums, and Experimental Bond Lengths

complex	ω_s (cm^{-1})	k_s (mdyn/Å)	bond	van der Waals radii (Å)[a]	exptl dist (Å)
O_3–C_2H_4	55.2	0.0318	C–O	3.17	3.24
O_3–C_2H_2[b]	59.7	0.0354	C–O	3.17	3.22
O_3–H_2O[c]	81.0	0.0506	O–O	3.00	3.17

[a] Assumed van der Waals radii of 1.5 Å for oxygen and 1.67 Å for carbon. [b] Reference 8. [c] Reference 29.

A recent ab initio and microwave spectral study of O_3–C_2H_2[8] finds that this related complex has a geometry remarkably similar to that of O_3–C_2H_4. The conformation is the same with the *a,c* symmetry plane bisecting the O–O–O angle of ozone and the C–C bond of acetylene. Ozone is tilted in the same sense with respect to the center of mass separation R_{cm} with a value of $\theta_1 = 112°$. Also, $R_{cm} = 3.25$ Å in O_3–C_2H_2, which is only 0.04 Å shorter than R_{cm} in O_3–C_2H_4.

An investigation of the SO_2–C_2H_4 complex has determined the conformation to be similar to that of O_3–C_2H_4 with an *a,c* symmetry plane, which bisects the O–S–O angle and the C=C bond in ethylene.[20] However, the SO_2 tilt is in the opposite sense with respect to R_{cm} than is that of ozone since $\theta_1 = 79.8°$ in SO_2–C_2H_4[20] and $\theta_1 = 112°$ in O_3–C_2H_4. This has the effect of placing the sulfur atom in SO_2 closest to the C=C bond in ethylene, while the two terminal oxygens of ozone are closest to the carbon atoms of ethylene. Unlike O_3–C_2H_4, the ethylene plane is parallel to the SO_2 plane since $\theta_2 = 110°$ for SO_2–C_2H_4.[20]

Only a few weakly bound ozone-containing bimolecular complexes are known. Table XI compares the van der Waals bond stretching force constant (k_s) and vibrational frequency (w_s) for O_3–C_2H_4, O_3–C_2H_2, and O_3–H_2O. These constants were estimated from the experimental values of the quartic centrifugal distortion constant (Δ_J) by means of the nonplanar asymmetric top equations developed by Millen.[28] The force constant and vibrational frequency for O_3–C_2H_4 are smaller than those for O_3–H_2O[29] and about equal to those for O_3–C_2H_2.[8] Qualitatively, this suggests that the van der Waals interaction is strongest for O_3–H_2O and about the same for O_3–C_2H_4 and O_3–C_2H_2. Comparison of the sum of van der Waals radii with the experimental bond distances appears to support a stronger van der Waals bond in O_3–H_2O. The sums of the van der Waals radii for oxygen and carbon (assuming 1.5 Å for oxygen and 1.67 for carbon) are smaller than the experimental C–O distances in O_3–C_2H_4 and O_3–C_2H_2, while the experimental O–O distance for O_3–H_2O[29] is almost the same as the sum of two oxygen van der Waal radii (see Table XI).

Two tunneling states have been observed for the three known bimolecular complexes containing ozone. In O_3–C_2H_4 and O_3–C_2H_2,[8] the tunneling splitting is small and the two states fit independently quite well to an asymmetric top Watson Hamiltonian. It appears that the internal motion involves rotation of ethylene or acetylene about a C_2 axis that is perpendicular to the molecular plane of ethylene or the molecular axis of acetylene. The ab initio calculation reported here estimates a barrier of 0.4 kcal/mol for the rotation of ethylene described above in O_3–C_2H_4. For O_3–H_2O,[29] the tunneling splitting is large and only one tunneling state fits to an asymmetric top Watson Hamiltonian, which suggests the barrier is quite low. In this case, water may undergo nearly free internal rotation.

For all three of these complexes, there is little information related to the motion of ozone and whether or not it is also involved in the tunneling splitting. An inversion of ozone that reverses the *c* dipole component of the complex can be ruled out since "rigid rotor" *c*-type transitions have been observed in the complexes. This is in contrast to Ar–O_3, where the *c*-type transitions are rotation–inversion and ozone inverts at a frequency of 460 MHz through a barrier of 50 cm^{-1}.[30]

A gearlike motion, which involves a concerted internal rotation of both ozone and the second monomer subunit, is possible for the three ozone-containing molecular complexes. The van der Waals complex SO_2–C_2H_4 exhibits two tunneling states, which are thought to arise from internal rotation of ethylene about the C_2 axis perpendicular to the molecular plane of ethylene.[20] Although this is similar to that of O_3–C_2H_4, there is oxygen-18 and

(28) Millen, D. J. *Can. J. Chem.* **1985**, *63*, 1477.
(29) Gillies, J. Z.; Gillies, C. W.; Suenram, R. D.; Lovas, F. J.; Schmidt, T.; Cremer, D. *J. Mol. Spectrosc.* **1991**, in press.
(30) (a) DeLeon, R. L.; Yokozeki, A.; Muenter, J. S. *J. Chem. Phys.* **1980**, *73*, 2044. (b) Muenter, J. S.; DeLeon, R. L.; Yokozeki, A. *Faraday Discuss. Chem. Soc.* **1982**, *73*, 63.

sulfur-34 data reported for SO_2–C_2H_4 that relates to the involvement of sulfur dioxide in the tunneling motion. The differences in the *A* rotational constants of the two tunneling states of $S^{18}O_2$–C_2H_4, $S^{18}O^{16}O$–C_2H_4, and $^{34}S^{16}O_2$–C_2H_4 decrease significantly in comparison to those of the normal isotopic species. It is possible that the reduction in the tunneling splitting observed for oxygen-18 and sulfur-34 isotopic substitution in sulfur dioxide may be due to a concerted gearlike motion, which exchanges the pair of equivalent oxygens as well as the two pairs of equivalent hydrogen nuclei. However, a motion that exchanges the oxygens and two pairs of hydrogens will give four tunneling states in $S^{18}O^{16}O$–C_2H_4, and only two states have been reported.[20] Unfortunately, the study of oxygen-18-substituted ozone complexes does not appear to be feasible.

Reaction Potential Surface. Ozone reacts with ethylene in the gas phase and in condensed media. The observation of a van der Waals complex between ethylene and ozone provides experimental structural data for a species located at large reactant distances along the reaction potential surface. The ab initio calculations and spectral data show that this complex is weakly bound and falls in a shallow minimum at large distances on the reaction surface. Scanning the potential energy surface (PES) of O_3–C_2H_4 by ab initio techniques reveals that the π complex (syn a form) is the most stable van der Waals complex between ozone and ethylene.[26b] Furthermore, the π complex is close to the transition state of the cycloaddition reaction between the two molecules and is located at the entrance to the cycloaddition reaction channel. This suggests that it is a precursor to the actual cycloaddition product, which means the stereochemical properties of reaction including product formation will be influenced by the stereochemistry in the π complex. Therefore, it is interesting to relate the geometry of the O_3–C_2H_4 π complex as obtained in this work to the geometry of the transition state and the product of the cycloaddition reaction.

Ozone adds to ethylene in a concerted fashion to give primary ozonide **1** as shown in eq 2. The addition is thermally allowed within the context of Woodward–Hoffman symmetry rules.[31-33] Maximal overlap between the π HOMO orbital of ethylene and the π^* LUMO orbital of ozone is achieved by a parallel plane approach to the two molecules.[31-33] As shown in Figure 6, this parallel plane orientation of the reacting ethylene and ozone maintains a symmetry plane along the reaction coordinate. It requires an oxygen envelope conformation with C_s symmetry for the transition state and the primary product **1** (see Figure 6).

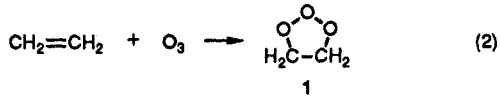

(2)

1

Ab initio calculations find the transition-state geometry to correspond to an oxygen envelope conformation with C_s symmetry.[26,34] Since the C–O distances in the transition state are calculated to be ~2.3–2.0 Å, the complex observed in the present work with C–O distances of 3.24 Å must fall on the reaction coordinate prior to the transition state. Recently we observed the primary product **1** in a low-temperature microwave absorption cell and found that the lowest energy gas-phase conformation is the oxygen envelope form with C_s symmetry.[13] Earlier ab initio calculations employing large augmented basis sets including polarization functions and complete geometry optimization predicted the oxygen envelope as the lowest energy conformation of **1** in accord with the gas-phase microwave results.[35]

The present results show that the O_3–CH_2=CH_2 complex also has the oxygen envelope conformation with C_s symmetry. Therefore, a combination of work supports the concerted addition of ozone to ethylene along the reaction coordinate predicted by 1,3-dipolar cycloaddition theory. The present work does not determine what role the observed complex plays in the reaction. It seems unlikely that the species exists in gas-phase ozone plus ethylene reactions at room temperature because the complex binding energy of 0.74 kcal/mol is too low. Detailed chemical dynamical studies that take advantage of the reactant orientation in the O_3–CH_2=CH_2 complex are needed to provide more critical tests of the concerted addition and symmetry requirements of 1,3-dipolar cycloaddition theory. Studies are underway in related cycloadditions that also use substituents to investigate van der Waals complexes and their possible roles in the observed regioselectivity of product formation.

Acknowledgment. D.C. and E.K. thank the Swedish Natural Science Research Council (NFR) for financial support and the Nationellt Superdatorcentrum (NSC), Linköping, Sweden, for a generous allotment of computer time. J.Z.G. is grateful to the Faculty Research Fund, Union College, for partial support of this research. All the ab initio calculations have been performed on the Cray XMP 48 of the NSC. We are grateful to Dr. J. T. Hougen and Dr. L. H. Coudert for helpful discussions related to the group theoretical aspects of the tunneling motion. This research was partially supported by a grant from Research Corp. to C.W.G.

(31) (a) Bailey, P. S. *Ozonation in Organic Chemistry*; Academic Press: New York, 1978; Vol. 1; 1982; Vol. 2. (b) Kuczkowski, R. L. *1,3-Dipolar Cycloadditions*; Padwa, A., Ed.; Wiley: New York, 1984; p 197.

(32) (a) Woodward, R. B.; Hoffman, R. *The Conservation of Orbital Symmetry*; Verlag Chemie GmSH: Weinheim, 1971. (b) Eckell, A.; Huisgin, R.; Sustmann, R.; Wallbillich, G.; Grashey, D.; Spindler, E. *Chem. Ber.* **1967**, *100*, 2192.

(33) (a) Sustmann, R. *Tetrahedron Lett.* **1971**, *29*, 2717. (b) Sustmann, R. *Pure Appl. Chem.* **1974**, *40*, 569. (c) Houk, K. N.; Sims, J.; Duke, R. E., Jr.; Strozier, R. W.; George, J. K. *J. Am. Chem. Soc.* **1973**, *95*, 7287. (d) Houk, K. N.; Sims, J.; Watts, C. R.; Luskus, L. J. *J. Am. Chem. Soc.* **1973**, *95*, 7301.

(34) Leroy, G.; Sana, M. *Tetrahedron* **1976**, *32*, 1379.

(35) Cremer, D. *J. Chem. Phys.* **1979**, *70*, 1911.